Journal of Engineering Mathematics (2006) 54: 345–358
DOI 10.1007/s10665-006-9039-0

A series-solution method for free-boundary problems arising from flow over topography

P.J. HIGGINS, W.W. READ and S.R. BELWARD
School of Mathematical and Physical Sciences, James Cook University, Townsville, Queensland, Australia (email: wayne.read@jcu.edu.au)

Received 16 December 2004; accepted in revised form 2 February 2006 / Published online: 14 April 2006

Abstract. An analytical series method is presented for steady, two-dimensional, irrotational flow of a single layer of constant-density fluid over topography. This problem is formulated as a Laplacian free-boundary problem with fully nonlinear boundary conditions. The method is an iterative scheme that allows the calculation of analytical series solutions for supercritical, transcritical and subcritical flow regimes over arbitrary topography. By an appropriate choice of the free-boundary representation, exponential convergence of the series solution is achieved. With this accuracy, the issue of apparent dual transcritical/subcritical solutions previously obtained by boundary-integral-equation methods (BIEM) is resolved. Results are compared with solutions previously obtained using BIEM, and solutions are presented for flow over asymmetric and arbitrarily shaped obstacles.

Key words: analytical series, arbitrary topography, exponential convergence, nonlinear solutions

1. Introduction

Flow over topography has been a topic of interest in the mathematical and physical sciences and engineering for many decades. Applications include flow in a channel and airflow over mountains. Early solution methods were dominated by linear theories. For example, Kelvin [1] studied flow in a channel obstructed by ridges or hollows, and Lamb [2, Section 249] calculated the drag on a cylindrical obstruction. Long [3] linearised the governing equations around uniform upstream flow of constant density and was able to obtain finite-amplitude-wave solutions. Submerged singularities have also been used to model flow over obstacles [4]. More recently, boundary-element methods have been used in conjunction with conformal mappings to calculate flow solutions for specific obstacles, such as semi-circles [5], semi-ellipses [6], a step [7] and a triangular weir [8].

Fully nonlinear flow over arbitrary topography was first examined by King and Bloor [9] who adopted a generalisation of the Schwarz-Christoffel transformation. An alternate method was presented by Belward and Forbes [10] who used a boundary-integral method in the original variables to compute downstream interfacial waves and single-layer transcritical flow. Belward [11] also calculated solutions for fully nonlinear flow over successive obstacles. Although some of these methods are theoretically capable of calculating flow solutions over asymmetric and arbitrary obstacles, few such solutions have been published to date.

In the case of irrotational and incompressible flow, the flow over topography problem reduces to solving Laplace's equation subject to nonlinear boundary conditions. The location of the upper surface is initially unknown, and it is along this free boundary that the nonlinearity occurs explicitly, although the entire problem can be considered nonlinear. Most

solution methods involve providing an initial guess for the position of the free surface which is updated at each iteration using a cost function based on one of the boundary conditions.

Purely numerical schemes such as boundary-integral and boundary-element methods have proved successful in solving these potential problems. But further computations are required in order to determine information about the fluid at interior points. The analytical series method presented in this paper has the advantage of efficiently producing continuous global solutions over the entire flow domain with exact error bounds immediately available. These methods have been used to solve steady saturated and unsaturated seepage problems on arbitrary flow domains by Read and Volker [12], or Gill and Read [13]. Note that in all these earlier problems, the free-boundary condition could be linearised.

In this paper, we present an iterative analytical series method for solving flow over an obstacle of finite length. We assume Laplacian flow, with fully nonlinear boundary conditions along the free surface. Three flow regimes are possible: supercritical, transcritical and subcritical flow. The subcritical solutions, characterised by a train of lee waves downstream of the obstacle, are the most difficult to calculate. The true test of success of a solution method is measured by its performance in the subcritical case. We will show that the analytical series method efficiently calculates accurate subcritical solutions with relative ease.

The convergence of the analytical series method may be enhanced, depending on specific aspects of its computation. For example, with the correct boundary representation, exponential convergence of the series solution is possible. This is a remarkable result given the difficulty researchers have had with this problem in the past.

With the increased efficiency and availability of error bounds we may investigate, with certainty, regions of the parameter space where solutions are difficult to calculate. For constant Froude number and increasing obstacle height, subcritical solutions exhibit waves of increasing amplitude. This behaviour continues until waves occur with a crest of 120°. At the same obstacle height it is possible to determine the Froude number for which transcritical flow occurs. Belward and Forbes [10] reported that transcritical and subcritical flows were possible at the same Froude number and obstacle height. This was in direct contrast to the work of Shen [14] whose weakly nonlinear theory showed that the transcritical flow solutions were a limiting case of subcritical flow. It is now apparent that the work of Belward and Forbes was misleading because of a lack of accuracy in their solution method, and that transcritical flow may indeed be a limiting case of subcritical flow. It is definitely the case that both solution types are not possible for the same obstacle height and Froude number.

A general theoretical framework for the analytical series method for known boundary problems is covered in full by Read [15] and is discussed briefly in Section 3. The representation of the free surface is an important issue. In Section 4 we show that, with the correct choice, exponential convergence of the series solution is possible. In Section 5 we examine the iterative update scheme, in particular the form of the cost function. Results are presented in Section 6, including comparisons with solutions from the boundary-integral approach. A selection of solutions for flow over asymmetric and arbitrarily shaped obstacles is also presented.

2. Mathematical formulation

We denote the velocity field throughout the flow region by $\mathbf{u}$ and the free surface by $y=\eta(x)$. If the fluid has a vertical height of H_0 upstream with a horizontal velocity of u_0, then the assumption of upstream uniform flow is written as

$$\eta(x)\to H_0 \quad \text{and} \quad \mathbf{u}\to u_0\mathbf{i} \quad \text{as} \quad x\to-\infty, \tag{1}$$

where **i** is the horizontal unit vector. Downstream of the obstacle we assume that flow quantities are bounded.

All variables are nondimensionalised in terms of H_0 and u_0, giving a uniform flow upstream with unit height and velocity. The remainder of this paper will contain nondimensionalised variables only. With these assumptions, the stream function $\Psi(x, y)$ satisfies Laplace's equation:

$$\nabla^2 \Psi = 0. \tag{2}$$

If we denote the bottom boundary by $y = f^b(x)$, then the assumptions that the free surface is a streamline, and that there is no penetration through the topography, give the top and bottom boundary conditions

$$\Psi(x, \eta(x)) = 1 \quad \text{and} \quad \Psi(x,\ f^b(x)) = 0. \tag{3}$$

The flow domain is truncated to a finite length $x \in [-s, s]$, where s is chosen large enough such that the flow continues to satisfy the above conditions. We will discuss suitable choices for the truncation parameter s in Section 6. With this truncation the side boundary conditions become

$$\Psi(-s, y) = y \quad \text{and} \quad \Psi(s, y) = \frac{y}{\eta_s}, \tag{4}$$

where η_s is the height of the fluid at $x = s$. Note that the condition at $x = s$ implies uniform mass flux, and is less restrictive than the corresponding condition ultimately employed in the boundary-integral method (see for example Equation (2.10) in Belward and Forbes [10]).

Within the fluid region, Euler's equation of motion is satisfied. As we only consider stationary solutions, time derivatives can be set to zero. Also, since the flow is irrotational, Euler's equation can be integrated to give the Bernoulli equation which is evaluated along the free surface $y = \eta(x)$ to give

$$\frac{1}{2} F_u^2 u^2 + \eta = \frac{1}{2} F_u^2 + 1, \tag{5}$$

where u is the magnitude of the velocity, F_u is the upstream Froude number defined by $F_u = u_0/\sqrt{g H_0}$, and g is acceleration due to gravity. The value of the Froude number largely determines the type of flow. Supercritical flow is wave-free and has $F > 1$ throughout the flow domain while transcritical flow, also wave-free, has $F < 1$ upstream of the obstacle and $F > 1$ downstream. Subcritical flow is typically characterised by a train of lee waves downstream of the obstacle and has $F < 1$ throughout the fluid system. The magnitude of the velocity at any point in the fluid can be expressed in terms of the stream function using

$$u^2 = \left(\frac{\partial \Psi}{\partial x}\right)^2 + \left(\frac{\partial \Psi}{\partial y}\right)^2. \tag{6}$$

Note that the velocity potential $\Phi(x, y)$ can be calculated from the stream function $\Psi(x, y)$ using the Cauchy-Riemann equations. We use the potential in an integrated form of the Bernoulli equation (see Section 5).

3. Analytical series method

The stream function $\Psi(x, y)$ is transformed to a related function $\psi(x, y)$ that satisfies homogeneous side boundary conditions at $x = \pm s$. The transformation is defined by

$$\Psi(x, y) = \psi(x, y) + y + \frac{(x+s)y}{2s}\left[\frac{1}{\eta_s} - 1\right]. \tag{7}$$

With this transformation $\psi(x, y)$ will also satisfy Laplace's equation:

$$\nabla^2\psi = 0, \tag{8}$$

subject to the homogeneous side boundary conditions

$$\psi(-s, y) = \psi(s, y) = 0, \tag{9}$$

and the transformed top and bottom boundary conditions

$$\psi[x, \eta(x)] = 1 - \eta(x) - \frac{(x+s)\eta(x)}{2s}\left[\frac{1}{\eta_s} - 1\right] = h^t(x), \tag{10}$$

$$\psi[x,\ f^b(x)] = -f^b(x) - \frac{(x+s)\,f^b(x)}{2s}\left[\frac{1}{\eta_s} - 1\right] = h^b(x). \tag{11}$$

The transformed velocity potential can be expressed as

$$\Phi(x, y) = \phi(x, y) + x + \frac{1}{4s}\left[(x+s)^2 - y^2\right]\left[\frac{1}{\eta_s} - 1\right]. \tag{12}$$

Once the transformed problem has been solved, a solution to the original problem is immediately available.

Applying the method of separation of variables allows the eigenvalues and eigenfunctions to be determined. The general solution can be expressed as

$$\psi(x, y) = \sum_{n=1}^{\infty} A_n u_n(x, y) + B_n v_n(x, y), \tag{13}$$

where

$$u_n(x, y) = \sinh\left(\frac{n\pi y}{2s}\right)\sin\left(\frac{n\pi(x+s)}{2s}\right), \tag{14}$$

$$v_n(x, y) = \cosh\left(\frac{n\pi y}{2s}\right)\sin\left(\frac{n\pi(x+s)}{2s}\right). \tag{15}$$

The transformed velocity potential has the form

$$\phi(x, y) = A_0 + \sum_{n=1}^{\infty} A_n \bar{u}_n(x, y) + B_n \bar{v}_n(x, y), \tag{16}$$

where

$$\bar{u}_n(x, y) = \cosh\left(\frac{n\pi y}{2s}\right)\cos\left(\frac{n\pi(x+s)}{2s}\right), \tag{17}$$

$$\bar{v}_n(x, y) = \sinh\left(\frac{n\pi y}{2s}\right)\cos\left(\frac{n\pi(x+s)}{2s}\right). \tag{18}$$

The series coefficients A_n and B_n are determined by invoking the upper and lower boundary conditions (10) and (11) which, using the above notation, we may express as

$$h^t(x) = \sum_{n=1}^{\infty} A_n u_n^t(x) + B_n v_n^t(x), \tag{19}$$

$$h^b(x) = \sum_{n=1}^{\infty} A_n u_n^b(x) + B_n v_n^b(x), \tag{20}$$

where $u_n^t(x) = u_n[x, \eta(x)]$, $u_n^b(x) = u_n[x, f^b(x)]$, $v_n^t(x) = v_n[x, \eta(x)]$ and $v_n^b(x) = v_n[x, f^b(x)]$. The series coefficients cannot be determined using the classical approach as the top and bottom boundary conditions are not constant. However, a relationship between the series coefficients can be determined by applying the principle of eigenfunction expansion to non-orthogonal basis functions. This process is covered in full by Read [15] and is discussed briefly here.

3.1. Evaluating the series coefficients

We assume that $\{v_i^b(x), i = 1, 2, \ldots\}$ from Equation (15) is a linearly independent set of vectors spanning a space of functions that includes $u_n^b(x)$ and $h^b(x)$. By expressing $u_n^b(x)$ and $h^b(x)$ in terms of this set, substituting the expansions in the bottom boundary condition (11) and rearranging, we get

$$B_n = k_n^{hb} - \sum_{i=1}^{\infty} A_i k_{ni}^{ub}, \quad n = 1, 2, \ldots \tag{21}$$

where k_{ni}^{ub} and k_n^{hb} are the expansion coefficients for $u_n^b(x)$ and $h^b(x)$, respectively. Carrying out the same procedure on the top boundary condition (10) gives a similar expression

$$B_n = k_n^{ht} - \sum_{i=1}^{\infty} A_i k_{ni}^{ut}, \quad n = 1, 2, \ldots \tag{22}$$

where k_{ni}^{ut} and k_n^{ht} are the expansion coefficients for $u_n^t(x)$ and $h^t(x)$, respectively. Eliminating B_n from (21) and (22) gives

$$\sum_{i=1}^{\infty} \left(k_{ni}^{ut} - k_{ni}^{ub}\right) A_i = k_n^{ht} - k_n^{hb}, \quad n = 1, 2, \ldots \tag{23}$$

Both sets of series coefficients are dependent on the expansion coefficients, which at this stage are unknown.

3.2. Evaluating the expansion coefficients

In practice, the series solution is truncated after an appropriate number of terms have been included. We assume N terms are sufficient to satisfy our accuracy criteria, and the truncation becomes an approximation to the infinite series:

$$\psi(x, y) \approx \psi_N(x, y) = \sum_{n=1}^{N} a_n u_n(x, y) + b_n v_n(x, y), \tag{24}$$

where a_n and b_n are the estimators of A_n and B_n, respectively. The truncated form of the velocity potential is

$$\phi(x,y) \approx \phi_N(x,y) = a_0 + \sum_{n=1}^{N} a_n \bar{u}_n(x,y) + b_n \bar{v}_n(x,y). \tag{25}$$

If we adopt the matrix notation $[\mathbf{a}]_n = a_n$ and $[\mathbf{b}]_n = b_n$, then after truncating the series, Equations (21) and (23) can be written as

$$\mathbf{b} = \mathbf{k}^{hb} - K^{ub}\mathbf{a} \quad \text{and} \quad (K^{ut} - K^{ub})\mathbf{a} = \mathbf{k}^{ht} - \mathbf{k}^{hb}, \tag{26}$$

where K^{ut}, K^{ub}, $\mathbf{k}^{ht}$ and $\mathbf{k}^{hb}$ are the expansion coefficient matrices defined by

$$\left[K^{ut}\right]_{ij} = k_{ij}^{ut}, \quad [K^{ub}]_{ij} = k_{ij}^{ub}, \quad [\mathbf{k}^{ht}]_j = k_j^{ht}, \quad [\mathbf{k}^{hb}]_j = k_j^{hb}, \tag{27}$$

for $i, j = 1, 2, \ldots, N$.

Read [15] first calculated the expansion coefficients using the orthogonality relationship which, in this case, first requires the Gram–Schmidt process to construct an orthonormal basis. Alternatively, least squares can simplify these calculations. But the majority of computational time in this formulation is taken up by calculating the inner-product integrals. Therefore, we replaced the inner products with a collocation method [16]. This procedure assumes that there are $L \geq N$ discrete evenly spaced points along the boundaries that satisfy the eigenfunction expansions exactly. Therefore

$$u_n^b(x_l) = \sum_{j=1}^{N} k_{nj}^{ub} v_n^b(x_l) \quad \text{and} \quad h^b(x_l) = \sum_{j=1}^{N} k_j^{hb} v_j^b(x_l), \tag{28}$$

for $n = 1, 2, \ldots, N$ and $l = 1, 2, \ldots, L$. In matrix notation, this becomes

$$U^b = V^b K^{ub} \quad \text{and} \quad \mathbf{h}^b = V^b \mathbf{k}^{hb}, \tag{29}$$

where

$$[U^b]_{ln} = u_n^b(x_l), \quad [V^b]_{ln} = v_n^b(x_l), \quad [h^b]_l = h^b(x_l). \tag{30}$$

A similar set of equations can be determined for the expansion coefficients for the top boundary. Once these matrix equations are solved for the expansion coefficients, the series coefficients in (26) can be determined. We have shown that, with the introduction of this collocation method, the efficiency of the entire solution process is increased by several orders of magnitude, with accuracy no worse than the full least-squares method [16].

3.3. Error estimates

The error in each solution is a combination of two factors: the truncation error in the series, and the errors in the top and bottom boundary conditions. The truncation error incurred by the series approximation is defined by $\epsilon_N(x,y) = \Psi(x,y) - \Psi_N(x,y)$. As Ψ and Ψ_N both satisfy Laplace's equation, so will $\epsilon_N(x,y)$ and therefore the maximum (and minimum) value of the potential function will occur on the flow boundaries [17, Section 2.2]. Thus, the accuracy of the flow solution is immediately available at each step of the iterative process by examining the root-mean-squared (RMS) error in the top and bottom boundary conditions (3), and the Bernoulli condition (5).

The RMS error ϵ_N^h in the approximation of a function $h(x)$ by $h_N(x)$ is given by

$$\epsilon_N^h = \left[\frac{1}{2s}\int_{-s}^{s}[h(x)-h_N(x)]^2\,\mathrm{d}x\right]^{\frac{1}{2}}, \tag{31}$$

where N is the number of terms used in the series. Note that ϵ_N^t is the absolute and relative error for the top boundary condition $\Psi[x,\eta(x)]=1$, and ϵ_N^b is the absolute error for the bottom boundary condition $\Psi[x, f^b(x)]=0$. As the Bernoulli equation must be satisfied along the free surface, we can also calculate the RMS error for the Bernoulli condition ϵ_N^B, where $h(x)=1+F_u^2/2$ and $h_N(x)=u_N(x,\eta(x))F_u^2/2+\eta(x)$. Similarly, we can calculate the error in the velocity potential along the top boundary using (12) and (25).

4. Boundary representations

During the solution process, the top boundary is iteratively updated at a set of knot points. Note that the density of update knot points is increased in areas of higher curvature. To define the top boundary between these points, an interpolant is constructed. The solution process is independent of the representation of the free surface, so an almost limitless choice of interpolants can be employed. The subcritical solutions require the most attention because of a more complicated profile in areas of high curvature. Figure 1 displays the top and bottom boundary errors for a typical subcritical solution as functions of the number of terms in the series for six different interpolants.

Clearly, the Fourier sine-series representation has a superior accuracy. If we assume that the errors in Figure 1 have the form $\epsilon_N = N^{-k}$ so that $\log\epsilon_N = -k\log N$, then k is approximately equal to 3·2 in the range $10 < N < 150$ for the sine-series representation of the top boundary. This increases to 7·7 if we consider the range $50 < N < 100$. Similarly, if we consider the sine-series representation of the bottom boundary, k is approximately equal to 3·0 for $N < 100$ and increases to 12·8 for $N > 100$. We believe that the slope of this line will continue to steepen and that we have exponential convergence in the series. The authors have discussed this further and given an explanation of why the sine-series representation performs so well [18].

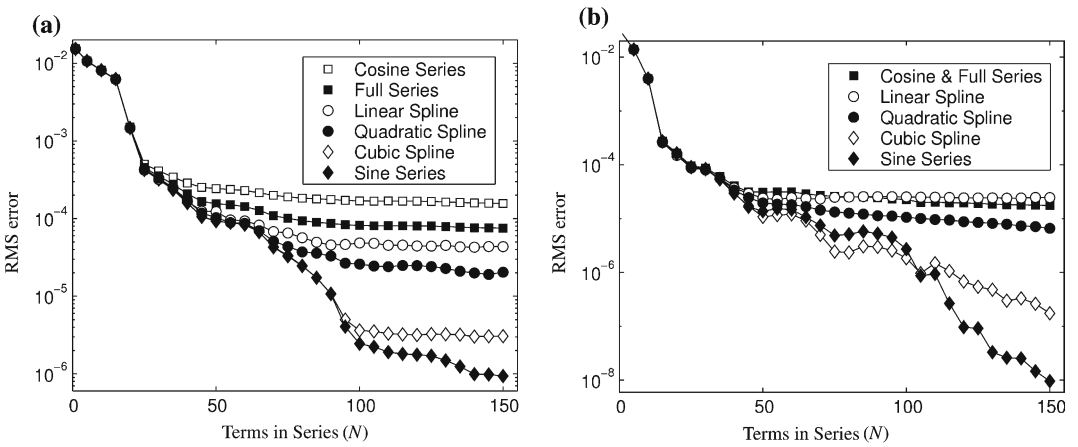

Figure 1. Semi-log plot of the RMS errors as a function of the number of terms in the series for six different boundary representations. (a) Top boundary. (b) Bottom boundary.

5. Iterative update scheme

The iterative process updates the top boundary $\eta(x)$ at each step by evaluating a cost function based on the Bernoulli equation (5). The update method has the form

$$\eta^{(i+1)}(x) = \eta^{(i)}(x) - c^{(i)}\delta\eta^{(i)}(x), \tag{32}$$

where i is the iteration count and $c^{(i)}$ is the multiplying factor which is chosen to enhance the convergence rate and takes the place of the inverse Jacobian in Newton's method. The free-boundary increment $\delta\eta^{(i)}(x)$ is calculated using a cost function.

The magnitude of the velocity along the free surface can be expressed as $u = \mathrm{d}\Phi/\mathrm{d}\zeta$ where $\mathrm{d}\zeta$ is measured along the streamline and $(\mathrm{d}\zeta)^2 = (\mathrm{d}x)^2 + (\mathrm{d}\eta)^2$. We integrate to give the velocity potential

$$\Phi = \int u\,\mathrm{d}\zeta = \int u\sqrt{1 + \left(\frac{\mathrm{d}\eta}{\mathrm{d}x}\right)^2}\,\mathrm{d}x. \tag{33}$$

Rearranging the Bernoulli condition (5) for the magnitude of the velocity along the free surface gives

$$u = \sqrt{\frac{2}{F_u^2}(1 - \eta(x)) + 1}. \tag{34}$$

Therefore the velocity potential can be expressed as

$$\Phi^B[x, \eta(x)] = \int_{-s}^{x} \left(\left[\frac{2}{F_u^2}(1 - \eta(x)) + 1 \right] \left[1 + \left(\frac{\mathrm{d}\eta}{\mathrm{d}x} \right)^2 \right] \right)^{\frac{1}{2}} \mathrm{d}x, \tag{35}$$

where the superscript B denotes the "Bernoulli" velocity potential. Using the series representation of the velocity potential in (12), we obtain that the integrated cost function has the form

$$C(x) = \Phi^B[x, \eta(x)] - \Phi_N[x, \eta(x)]. \tag{36}$$

Using this formulation, we calculated solutions for all three flow regimes for a large range of obstacle heights and Froude numbers.

6. Results

The analytical series method is very flexible; however, the accuracy of each solution is affected by many factors. In particular, we note four parameters: the number of terms in the series solution, the number of update knot points, the number of terms in the Fourier-series approximation, and the number of collocation points used to calculate the expansion coefficients. These values must be chosen to ensure a high level of accuracy while minimising computational time.

The choice of truncation parameter s is not overly important in the solution process provided that the obstacle is well within the interval $[-s, s]$. The assumption of uniform mass flux downstream is remarkably robust even for the wave solutions, particularly when s is chosen to be midway between the trough and crest of a wave where there is no perceptible deformation of the wave. When s is near a trough or crest, the computed η is inaccurate over the

last wave. When this occurs, we remove the last wave from the solution. Figure 2 shows superimposed wave solutions for an obstacle height $h = 0{\cdot}1$ with $s = 1, 2, \ldots, 17$ and $F_u = 0{\cdot}5$.

The standard bottom boundary that we used consists of a symmetric cosine-shaped obstacle with half base length of l and maximum height of h, and is defined by

$$f^b(x) = \begin{cases} \frac{h}{2}\left[\cos(\pi x/l) + 1\right], & -l \le x \le l \\ 0. & -s \le x \le -l \text{ and } l \le x \le s \end{cases} \tag{37}$$

Figure 3 contains a selection of transcritical and subcritical solutions for symmetric cosine shaped obstacles with different heights.

These figures show that the analytical series method is correctly predicting the general characteristics of each flow regime. That is, the hydraulic fall is deeper for higher obstacles during transcritical flow, and the amplitude of the downstream waves is larger for higher obstacles during subcritical flow.

6.1. Comparing analytical series and boundary-integral methods

We will compare the solutions we have calculated with those determined by Belward and Forbes [10] using BIEM. Figure 4 compares a single subcritical solution calculated using the analytical series method and a solution calculated using BIEM.

We see that both profiles possess the same general characteristics. However, the solution calculated using the analytical series method does not possess spurious upstream waves. The presence of the upstream waves in the BIEM solutions is known to be caused by slightly inadequate boundary conditions employed at $x = -s$ [10]. Note also the analytical series solution has a larger wave amplitude downstream. This could possibly be explained as a cancellation effect between the upstream waves in the BIEM solution interacting with the waves produced by the obstacle.

Table 1 displays the RMS errors for a single transcritical and subcritical solution calculated by each method. Note that we were supplied with the free-surface knot points of the BIEM solutions. To calculate the BIEM errors we carried out exactly the same process as for the series solutions. That is, we used the knot points to construct a cubic spline so that the evenly spaced collocation points could be determined. Then we represented the free surface by a Fourier sine series and used the analytical series method to calculate the errors required for the comparison.

We note that all errors are lower for the analytical series method. The most significant difference is observed when comparing errors in the Bernoulli condition for the subcritical solutions. The analytical series method has an error two orders of magnitude lower than the implementation of BIEM by Belward and Forbes. The same observation was made for all obstacle heights.

We now compare the range of obstacle heights for which each method was capable of calculating solutions. Note that, for each obstacle, there exists a single transcritical flow solution with a unique upstream Froude number. We observed very little difference in the Froude number calculated for each obstacle height when comparing the two methods. These values are displayed by the single solid line in Figure 5. The shaded region and the region below the dashed line represent the subcritical solutions calculated by the analytical series method and BIEM, respectively.

We observe that BIEM calculates both transcritical and subcritical solutions for some obstacles at the same Froude number (*i.e.*, the solid line crosses the dashed line). This is in direct contrast to the theory of Shen [14] and was not the case with the analytical series

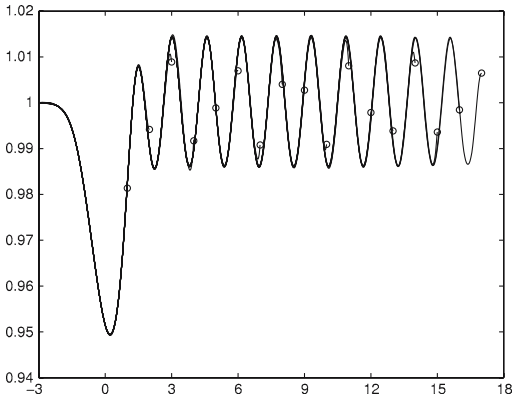

Figure 2. Superimposed subcritical solutions for various base lengths s. The limits of the flow domain are marked with a ○.

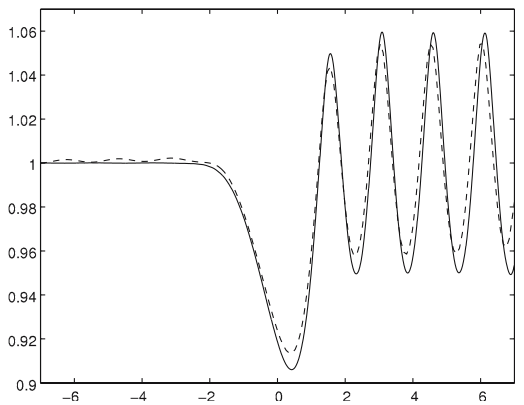

Figure 4. A comparison of subcritical flow solutions over a relatively large obstacle. Solid line: analytical series method. Dashed line: boundary-integral method. $s=7{\cdot}0, l=2{\cdot}0, h=0{\cdot}141, F_u=0{\cdot}5$.

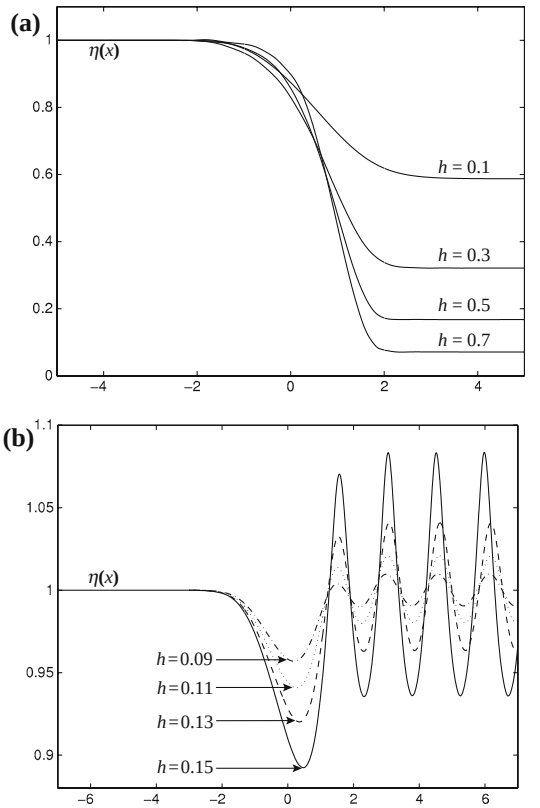

Figure 3. Examples of flow over symmetric obstacles. In (a) Critical flow, $s=5{\cdot}0$, $l=2{\cdot}0$, and in (b) Subcritical flow, $s=7.0$, $l=2{\cdot}0$, $F_u=0{\cdot}5$.

Table 1. RMS errors in the Bernoulli condition (ϵ_N^B), the top boundary (ϵ_N^t) and the bottom boundary (ϵ_N^b) for a transcritical and subcritical solution calculated by the analytical series method and BIEM.

	ϵ_N^B	ϵ_N^t	ϵ_N^b
Transcritical solutions ($s=5{\cdot}0$, $l=2{\cdot}0$, $h=0{\cdot}5$, $F\approx0{\cdot}22$)			
Analytical Series	$1{\cdot}64\times10^{-2}$	$2{\cdot}26\times10^{-4}$	$2{\cdot}09\times10^{-4}$
BIEM	$3{\cdot}39\times10^{-2}$	$3{\cdot}42\times10^{-4}$	$2{\cdot}10\times10^{-4}$
Subcritical solutions ($s=7{\cdot}0$, $l=2{\cdot}0$, $h=0{\cdot}141$, $F_u=0{\cdot}5$)			
Analytical Series	$7{\cdot}28\times10^{-5}$	$1{\cdot}85\times10^{-5}$	$1{\cdot}44\times10^{-6}$
BIEM	$4{\cdot}52\times10^{-3}$	$1{\cdot}88\times10^{-5}$	$1{\cdot}45\times10^{-6}$

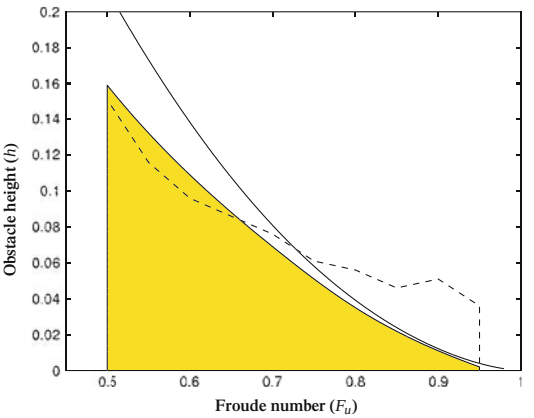

Figure 5. Obstacle heights for which solutions could be calculated for Froude numbers in the range $0{\cdot}5 \leq F_u \leq 0{\cdot}95$. Solid line: analytical series and BIEM critical solutions. Shaded region: analytical series subcritical solutions. Region surrounded by dashed line: BIEM subcritical solutions.

method. Because of the significant increase in accuracy with the analytical series method, we conclude that there are no obstacle heights that have both transcritical and subcritical flow solutions at the same Froude number. This does not contradict the weakly nonlinear theory proposed by Shen [14].

6.2. Flow over asymmetric obstacles

The standard form that we used for a bottom boundary containing an asymmetric obstacle with a maximum height of h, an upstream base length of l_1 and a downstream base length of l_2 is given by

$$f^b(x) = \begin{cases} \frac{h}{2}\left[\cos(\pi x/l_1)+1\right], & -l_1 \leq x \leq 0 \\ \frac{h}{2}\left[\cos(\pi x/l_2)+1\right], & 0 \leq x \leq l_2 \\ 0, & \text{otherwise.} \end{cases} \tag{38}$$

Figure 6 displays supercritical, transcritical and subcritical flow solutions over asymmetric obstacles.

The supercritical solutions in Figure 6(a) show that, although the obstacle is significantly skewed, the resulting free surface is close to symmetric. We have also seen that, for flow over a symmetric obstacle, the point at the maximum height of the supercritical solution has the same x-coordinate as the point at the maximum height of the obstacle. Here we see that the highest point of the free surface over the asymmetric obstacle does not coincide with the highest point of the obstacle.

Figure 6(b) shows that, although the transcritical flow solutions over asymmetric obstacles are uniform downstream, they have different heights and therefore different velocities. Also, we note that the asymmetry of the obstacle causes a significant difference in the heights of the three free-surface profiles directly above the obstacle ($-2{\cdot}0 < x < 2{\cdot}0$).

The most interesting of these is the subcritical solutions in Figure 6(c). Here we see that the amplitude of the waves downstream of the asymmetric obstacles are significantly larger than the amplitude for the flow over the symmetric obstacle. We also note that downstream of the obstacle the two asymmetric solutions coincide with each other and are both approximately a half wavelength out of phase with the symmetric flow.

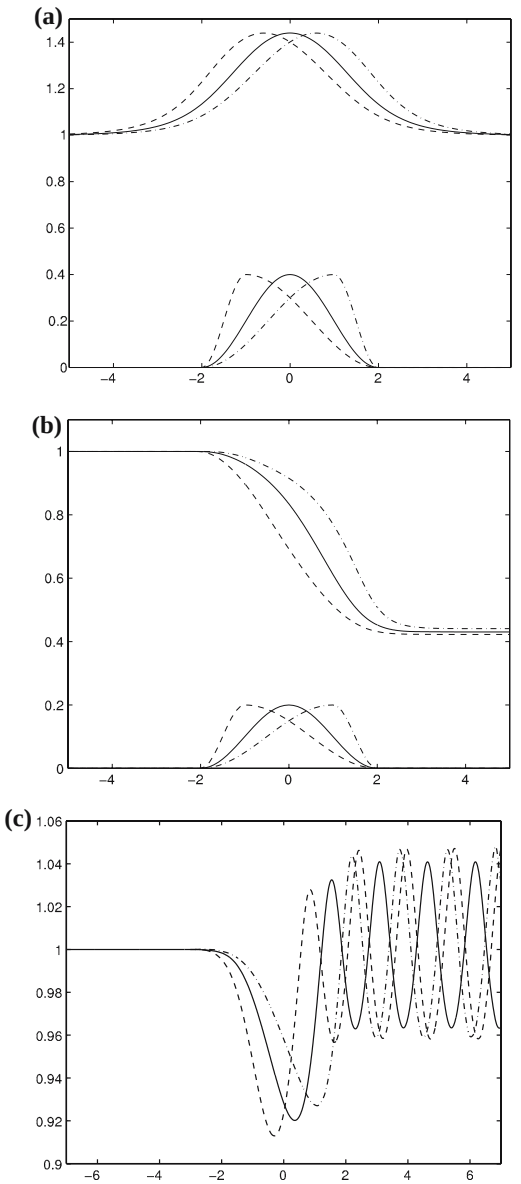

Figure 6. Comparisons of flow over symmetric and asymmetric obstacles. In (a) Supercritical flow, $s = 5{\cdot}0$, $h = 0{\cdot}4$, $F_u = 1{\cdot}7$, in (b) Critical flow, $s = 5{\cdot}0$, $h = 0{\cdot}2$, and in (c) Subcritical flow, $s = 7{\cdot}0$, $h = 0{\cdot}13$, $F_u = 0{\cdot}5$. (Solid: $l_1 = l_2 = 2$, Dashed: $l_1 = 1$, $l_2 = 3$, Dot-dashed: $l_1 = 3$, $l_2 = 1$).

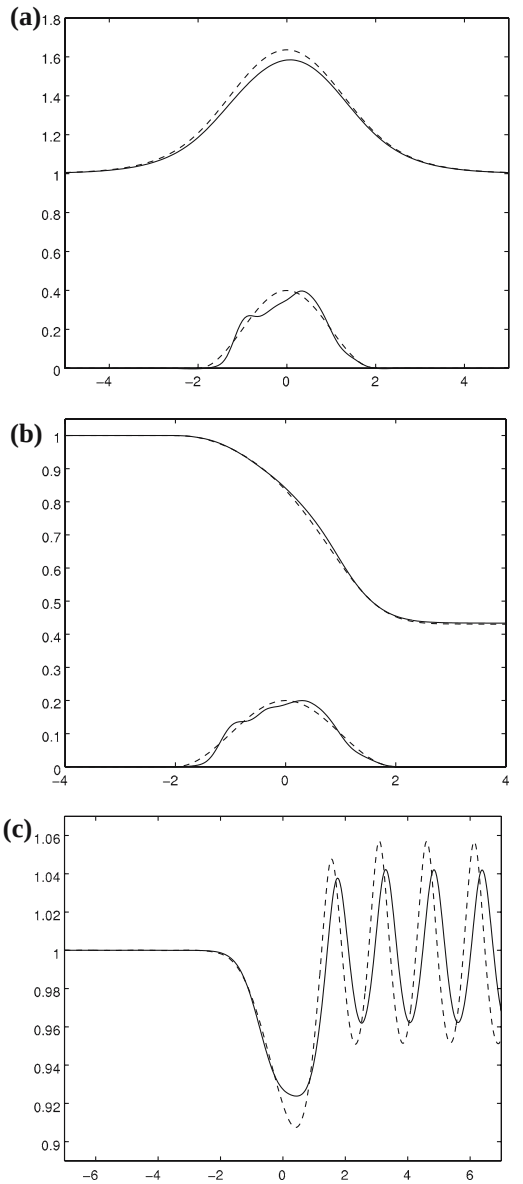

Figure 7. Examples of flow over arbitrary (solid line) and symmetric (dashed line) obstacles. In (a) Supercritical flow, $s = 5{\cdot}0$, $l = 2{\cdot}0$, $h = 0{\cdot}4$, $F_u = 1{\cdot}7$, in (b) Critical flow, $s = 4{\cdot}0$, $l = 2{\cdot}0$, $h = 0{\cdot}2$, and in (c) Subcritical flow, $s = 7{\cdot}0$, $l = 2{\cdot}0$, $h = 0{\cdot}14$, $F_u = 0{\cdot}5$.

6.3. Flow over arbitrary obstacles

Another interesting application for the analytical series method is flow over arbitrary topography. The bottom boundary we used was obtained by vertically moving the knot points of a symmetric cosine-shaped obstacle. Although each point was moved by an arbitrary distance, the general shape of the obstacle is preserved. Increasing the maximum distance a point is allowed to move will increase the complexity of the topography. The evenly spaced

knot points are used as collocation points to calculate the Fourier-series coefficients for the bottom boundary representation. Figure 7 displays supercritical, transcritical and subcritical flow solutions over arbitrary shaped obstacles.

Figure 7(a), shows that supercritical flow over the arbitrary obstacle is similar to the flow over an asymmetric obstacle (Figure 6(a)), in that the solution is slightly skewed towards the point of maximum obstacle height. We note that, although the obstacles have the same maximum height, the resulting free surfaces have a significant difference in maximum height.

Figure 7(b) shows that transcritical flow over the arbitrary obstacle is very close to the flow over the symmetric obstacle. We note that there is a small difference in the height of the flow downstream, and that there exists a "bump" in the profile above the point of maximum height of the arbitrary obstacle.

From the subcritical solutions in Figure 7(c), we see that there is a significant difference in the initial drop of the fluid that occurs above the obstacle ($x \approx 0$), and in the amplitude of the downstream waves that have also experienced a horizontal shift.

7. Discussion and conclusions

In this paper, analytical series solutions for two-dimensional, single-layer fluid flow over topography have been presented. The solution process consists of iteratively updating the position of the free surface by evaluating a cost function. The updated top boundary effectively reduces the Laplacian free-boundary problem to a regular known boundary problem at each step. A new set of series coefficients is then calculated using the principle of eigenfunction expansions to define the updated solution. Error measurements are immediately available for use as convergence criteria for the update method. This procedure was used to calculate supercritical, transcritical and subcritical flow solutions over symmetric, asymmetric and arbitrarily shaped obstacles.

An important feature of the solution technique is the method used to represent the top and bottom boundaries. The solution process is independent of the boundary representation, so we have an almost limitless choice of interpolant. We displayed the convergence rates for six different interpolants, and showed that exponential convergence in the series solution is possible using a Fourier sine-series representation of the boundaries.

The analytical series method was used to calculate flow solutions over asymmetric and arbitrarily shaped obstacles. Our results suggest a strong relationship between the skewness of the obstacle and the horizontal position of the downstream waves during subcritical flow. Also, the wavelength did not appear to be affected by the skewness, but the amplitude of the waves was significantly altered.

Solutions for flow over symmetric obstacles were compared with those calculated previously by the boundary-integral method. It was observed that the RMS errors in the solutions calculated with the analytical series method were consistently lower than this implementation of BIEM. A difference of two orders of magnitude was observed in the errors for the Bernoulli condition during subcritical flow, arguably the most difficult flow regime to solve. Another difference was observed when examining the maximum obstacle height possible for a stable subcritical solution. BIEM calculated a range of dual transcritical/subcritical solutions for a single obstacle. Because of the accuracy of the analytical series method, we conclude that there is no basis for accepting the earlier conclusion that there are obstacles that have both a transcritical and subcritical flow solution.

We are currently extending the series method to more realistic atmospheric models. In particular, non-Laplacian flows resulting from isothermal or linear-temperature-decay

atmospheric models are being computed. In addition to this the efficiency and accuracy of the series method allows us to extend our computations to the three-dimensional version of any of these problems. We will be presenting these results in future publications.

References

1. W. Kelvin, On stationary waves in moving water. *Phil. Mag.* 22 (1886) 353–357.
2. H. Lamb, *Hydrodynamics, 6th ed*. Cambridge: Cambridge University Press (1932) 738 pp.
3. R.R. Long, Some aspects of the flow of stratified fluids, I. A theoretical investigation. *Tellus* 5 (1953) 42–58.
4. J.V. Wehausen and W.V. Laitone, Surface waves. In: S. Flügge (ed.), *Handbuch der Physik*, Vol. 9. Heidelberg: Springer (1960) pp. 446–778.
5. L.K. Forbes and L.W. Schwartz, Free-surface flow over a semicircular obstruction. *J. Fluid Mech.* 114 (1982) 299–314.
6. L.K. Forbes, On the wave resistance of a submerged semi-elliptical body. *J. Engng. Math.* 15 (1982) 287–298.
7. A.C. King and M.T.G. Bloor, Free surface flow over a step. *J. Fluid. Mech.* 182 (1987) 193–208.
8. F. Dias and J.M. Vanden-Breock, Open channel flows with submerged obstructions. *J. Fluid. Mech.* 206 (1989) 155–170.
9. A.C. King and M.T.G. Bloor, A Semi-inverse method for free surface flow over a submerged body. *Quart. J. Mech. Appl. Math.* 42 (1989) 183–202.
10. S.R. Belward and L.K. Forbes, Interfacial waves and hydraulic falls: some applications to atmospheric flows in the lee of mountains. *J. Engng. Math.* 29 (1995) 161–179.
11. S.R. Belward, Fully nonlinear flow over successive obstacles: hydraulic fall and supercritical flows. *J. Austral. Math. Soc. Ser. B.* 40 (1999) 447–458.
12. W.W. Read and R.E. Volker, Series solutions for steady seepage through hillsides with arbitrary flow boundaries. *Water Resources Res.* 29 (1993) 2871–2880.
13. A.W. Gill and W.W. Read, Efficient analytic series solutions for two-dimensional potential flow problems. *Int. J. Numer. Meth. Fluids* 23 (1996) 415–430.
14. S.S.P. Shen, Forced solitary waves and hydraulic falls in two-layer flows. *J. Fluid Mech.* 234 (1992) 583–612.
15. W.W. Read, Series solutions for Laplaces equation with nonhomogeneous mixed boundary conditions and irregular boundaries. *Math. Comput. Model.* 17 (1993) 9–19.
16. W.W. Read, S.R. Belward and P.J. Higgins, An efficient iterative scheme for series solutions to Laplacian free boundary problems. *ANZIAM J.* 44 (2003) C644–C663.
17. D. Gilbarg and M.S. Trudinger, *Elliptic Partial Differential Equations of Second Order, 2nd ed*. Berlin: Springer (1983) 530 pp.
18. S.R. Belward, W.W. Read and P.J. Higgins, Efficient series solutions for non-linear flow over topography. *ANZIAM J.* 44 (2003) C96–C113.